IOP Publishing Journal of Physics G: Nuclear and Particle Physics

J. Phys. G: Nucl. Part. Phys. **47** (2020) 055113 (17pp) https://doi.org/10.1088/1361-6471/ab6f1d

Ab initio no-core shell model study of $^{18-23}$O and $^{18-24}$F isotopes

Archana Saxena and Praveen C Srivastava[1]

Department of Physics, Indian Institute of Technology Roorkee, Roorkee 247 667, India

E-mail: archanasaxena777@gmail.com and pcsrifph@iitr.ac.in

Received 12 August 2019, revised 23 December 2019
Accepted for publication 23 January 2020
Published 9 April 2020

Abstract

In the present work, we have done a comprehensive study of the low-lying energy spectrum for oxygen and fluorine chains using an *ab initio* no-core shell model. We have used an inside-nonlocal outside-Yukawa (INOY) potential, which is a two-body interaction but also has the effect of three-body forces via short range and nonlocal character. Also, we have performed calculations with N3LO and N^2LO_{opt} interactions and compared corresponding results with the experimental data and phenomenological USDB interaction. We have reached up to $N_{max} = 6$ for $^{18-21}$O and $^{18-19}$F, $N_{max} = 4$ for other oxygen and fluorine isotopes, respectively. We have also discussed the binding energy of oxygen and fluorine chains. Over binding in the ground state (g.s.) energy in neutron rich oxygen isotopes is observed in our largest model space calculations.

Keywords: *Ab initio*, drip-line, no-core shell model

(Some figures may appear in colour only in the online journal)

1. Introduction

Recent developments in computing power have made it possible to study the nuclei beyond the *p* shell using the no-core shell model (NCSM) approach [1–9]. The NCSM is a basic tool for explaining the nuclear structure and nuclear bound state problems, which uses nuclear interactions from first principles. Now, calculations are also available with the continuum effect in NCSM for explaining unbound states, scattering and nuclear reactions. Recently, NCSM calculations with the continuum effect for ^{11}Be have been performed; the parity inversion problem is solved for ^{11}Be using the NCSM approach [10–12] with chiral

[1] Author to whom any correspondence should be addressed.

interaction N^2LO_{SAT} [13]. *Ab initio* approaches give us an opportunity to calculate the electromagnetic properties of exotic nuclei more precisely [14]. The NCSM calculations have various applications in nuclear structure as well as in nuclear reaction physics. New physics is coming out, e.g. $N = 8$ magic number is no longer a magic number when we increase neutron and proton ratio. There is another method known as the no-core shell model, with a core constructed for the heavier nuclei [1, 15–21]. To understand the details of fully open shell medium mass nuclei from first principles is still a challenge. Research for open shell nuclei is still going on using many *ab initio* approaches [22, 23]. The study of neutron rich nuclei from first principles is an interesting topic nowadays. The exact location of the drip line in neutron rich oxygen isotopes can be explained by *ab initio* approaches using NN+3N(full) chiral interactions where the role of 3N forces is very important [24]. The no-core shell model with perturbation approach (NCSM-PT) results for low-lying states in $^{18-20}$O isotopes are reported in [23].

In the present work our aim is to systematically study the low-lying energy spectrum (positive parity) for oxygen ($^{18-23}$O) and fluorine ($^{19-24}$F) chains using an *ab initio* no-core shell model. For the first time we have reached up to $N_{\max} = 6$ calculations for $^{18-21}$O and ^{18,19}F isotopes.

The paper is organized as follows: in sections 2 and 3, the NCSM and its formalism are given. The effective interactions used in calculations are described in section 4. Results and discussions are reported in section 5. Neutron drip line in oxygen isotopes is discussed in section 6. Finally the paper is concluded in section 7.

2. *Ab initio* No-Core Shell Model

The *ab initio* no-core shell model [2, 3] is a many-body approach which is used to solve the full *A*- body Hamiltonian. No core is assumed in this model; all the nucleons are treated as active non-relativistic pointlike particles interacting with realistic *NN* or *NN* + *NNN* interactions which fit Nijmegan *NN* phase shifts up to an energy of 350MeV with a very high precision. However, in the shell model, we assume a core, so, the core particles are considered to be inactive. For NCSM, we choose the Harmonic Oscillator (HO) basis for the calculations because in this we can use a second quantization formalism and our system remains translationally invariant. The *NN* potentials which generate short range correlations cannot be accommodated in the HO basis for e.g. Argonne V18(AV18) [25], CD-Bonn 2000 [26] and INOY [27, 28] potentials. Chiral potentials [29] also produce short range correlations up to some extent. To accommodate these correlations and speeding up the convergence with the expansion of basis, we need an effective interaction from starting realistic *NN* and *NN* + *NNN* interactions. Effective interactions can be generated by using unitary transformation. Many soft potentials (which do not generate short range correlations) are also available nowadays for e.g. V_{lowk} [30], SRG *NN* [31] etc. In the present work, we have also compared our NCSM results with phenomenological USDB effective interaction [32].

3. Formalism

We have to solve the A-body Schrödinger equation. The starting Hamiltonian is given as

$$H_A = T_{rel} + V = \frac{1}{A}\sum_{i<j}^{A}\frac{(\vec{p}_i - \vec{p}_j)^2}{2m} + \sum_{i<j}^{A} V_{NN,ij} \tag{1}$$

where m is the mass of the nucleon and A is the number of nucleons (i.e., the mass number). The first term is relative kinetic energy defined in terms of momenta of each nucleon ($p_{i,j} = 1, 2, 3 \ldots A$), and the second term is nucleon-nucleon NN interaction which has a nuclear as well as a Coulomb part. We modify equation (1), by adding the HO center-of-mass term $H_{CM} = T_{CM} + U_{CM}$, where $U_{CM} = \frac{1}{2}Am\Omega^2\vec{R}^2$, $\vec{R} = 1/A\sum_{i=1}^{A}\vec{r}_i$ and Ω is the HO frequency.

$$H_A^{\Omega} = H_A + H_{CM} = \sum_{i=1}^{A} h_i + \sum_{i<j}^{A} V_{ij}^{\Omega,A} = \sum_{i=1}^{A}\left[\frac{\vec{p}_i^{\,2}}{2m} + \frac{1}{2}m\Omega^2\vec{r}_i^{\,2}\right] + \sum_{i<j}^{A}\left[V_{NN,ij} - \frac{1}{2A}m\Omega^2(\vec{r}_i - \vec{r}_j)^2\right]. \tag{2}$$

In the final calculations the CM term will be subtracted out. The new Hamiltonian breaks into two parts, one-body and two-body parts. Now, we divide our basis space into two parts, one in which we do the calculations, called P model space, which is finite. The second one is Q ($=1 - P$) model space, which is excluded space. Since the Harmonic-oscillator basis is infinite, we make a truncation in the Q space (see [33] for more details).

These operators satisfy the conditions $P^2 = P$, $Q^2 = Q$, $PQ = 0$, and $P + Q = 1$. We introduce an operator, ω, which is a transformation operator of similarity transformation of the Hamiltonian $e^{-\omega}He^{\omega}$, satisfies the condition $\omega = Q\omega P$. This operator acts as a mapping between the P and Q spaces. The eigenstates of initial Hamiltonian can be denoted by $|k\rangle$ with eigenvalues E_k.

$$H|k\rangle = E_k|k\rangle. \tag{3}$$

The basis states of P and Q spaces are expressed as $|\alpha_P\rangle$ and $|\alpha_Q\rangle$. The $|\alpha_P\rangle$ belongs to $|\alpha_Q\rangle$ and follow the relation $Qe^{-\omega}He^{\omega}P = 0$. The $|\alpha_Q\rangle$ states can be expressed in terms of $|\alpha_P\rangle$ states with the help of ω operator[34],

$$\langle\alpha_Q|k\rangle = \sum_{\alpha_P}\langle\alpha_Q|\omega|\alpha_P\rangle\langle\alpha_P|k\rangle. \tag{4}$$

The operator ω can be found out from equation (4). Let d_P be the dimension of model space P and $\mathscr{K}$ be a set of the d_P eigen vector vectors which satisfies the relation 4. The $d_P \times d_P$, which is a matrix having matrix elements $\langle\alpha_P|k\rangle$ for $|k\rangle \in \mathscr{K}$ is invertible, under this condition the operator ω,

$$\langle\alpha_Q|\omega|\alpha_P\rangle = \sum_{k\in\mathscr{K}}\langle\alpha_Q|k\rangle\langle\tilde{k}|\alpha_P\rangle, \tag{5}$$

where tilde denotes the matrix elements of the inverse matrix $\langle\alpha_P|k\rangle$, e.g., $\sum_{\alpha_P}\langle\tilde{k}|\alpha_P\rangle\langle\alpha_P|k'\rangle = \delta_{k,k'}$, for $k, k' \in \mathscr{K}$.

For model space P, the Hermitian effective Hamiltonian is given by

$$\bar{H}_{eff} = [P(1 + \omega\dagger\omega)P]^{1/2}PH(P + Q\omega P)[P(1 + \omega\dagger\omega)P]^{-1/2}. \tag{6}$$

This Hamiltonian can be rewritten by using properties of the ω operator

$$\bar{H}_{eff} = [P(1 + \omega\dagger\omega)P]^{-1/2}(P + P\omega\dagger Q)H(Q\omega P + P)[P(1 + \omega\dagger\omega)P]^{-1/2}. \tag{7}$$

We need effective interactions to employ in our model space because of the short range repulsive nature of realistic NN interactions. For this purpose, we perform a unitary transformation. We apply unitary transformation to equation (2) such that the model space P and Q are decoupled from each other [35, 36]. After applying unitary transformation we get the Hermitian effective interaction $H_{eff} = Pe^{-S}H_A^{\Omega}e^{S}P$. H_{eff} is an A-body operator. In our approximation the Hamiltonian is at two-body cluster level, for details, see [1, 14]. We have

following variational parameters in the final Hamiltonian; first one is the harmonic oscillator frequency $\hbar\Omega$, the second one is nucleon number A and third one is the size of the model space $N_{\max}$, where $N_{\max}$ is the parameter that measures the maximal allowed HO excitation energy above the unperturbed ground state. When $N_{\max} \to \infty$, $V_{ij,eff}^{\Omega,A} \to V_{ij}^{\Omega,A}$. So, as we increase model space, the dependency on Ω decreases and we get the converge result. In NCSM, effective interactions are translationally invariant. Because of this we can decouple the c.m. components from all observables. Our effective Hamiltonian is in A-body space. To construct this, we subtract the c.m. Hamiltonian and add the Lawson projection term [37] $\beta(H_{c.m.} - \frac{3}{2}\hbar\Omega)$ to shift spurious states which comes because of c.m. excitations. In the present work we have taken β=10. The eigenvalues of physical states are independent of β. Now the effective Hamiltonian (equation (8)) is given as:

$$H_{A,eff}^{\Omega} = P\left\{\sum_{i=1}^{A}\left[\frac{(\vec{p}_i - \vec{p}_j)^2}{2mA} + \frac{m\Omega^2}{2A}(\vec{r}_i - \vec{r}_j)^2 + V_{ij,eff}^{\Omega,A}\right] + \beta\left(H_{c.m.} - \frac{3}{2}\hbar\Omega\right)\right\}P. \tag{8}$$

Computationally, obtaining the eigenvalues of the many-body Hamiltonian is not an easy task because it involves a very huge matrix to diagonalize. In the present paper we have used the pANTOINE [38–40] shell model code which is adapted to NCSM [41]. The NCSM is a sparse matrix eigenvalue problem. The dimensions of the Hamiltonian matrix increases with atomic number A and increasing $N_{\max}$. In the case of heavier neutron rich O and F isotopes, the dimensions are very large. Thus, we have performed calculations up to $N_{\max} = 4$ only. In our calculations, in the case of ^{21}O, corresponding to $N_{\max} = 6$, dimension is $\sim 3.36 \times 10^9$; for ^{19}F, corresponding to $N_{\max} = 6$, dimension is $\sim 1.35 \times 10^9$.

4. Effective *NN* interaction

In NCSM, as we increase model space size, solving the many-body problem becomes computationally hard. We want to do calculations with *NN* interactions in the maximum model space size. Previously, the INOY interaction is used in NCSM calculations to find the binding energies, excited states of both parities, electromagnetic moments, and point-nucleon radii in Be isotopes [14].

There are two reasons behind choosing the INOY potential. The first one is that it contains a three-body effect through nonlocality in some partial waves so we get the effect of three-body forces without adding three-body forces explicitly, and the second reason is that we get fast convergence for the INOY interaction for a given $N_{\max}$ in comparison to any other interaction. The nonlocality and three-body forces are deeply related to each other [42]. The INOY potential is a nonlocal potential in a coordinate space. Actually it is a mixture of local and nonlocal parts, local Yukawa tail at longer ranges (>3 fm) and nonlocal at short range. As we know nucleons have internal structure, because of this a nonlocality character comes at short range (up to 1–1.5 fm). The INOY *NN* interaction (set of $^1S_0$ and $^3SD_1$ *NN* interactions) is in coordinate space and it was constructed to see the effect on triton binding energy. When we use the coordinate space, it is easy to handle the ranges of local and nonlocal parts explicitly. In coordinate space, because of the basic property (short range nature) of *NN* interaction, it should vary as an exponential function at long ranges.

The form of the INOY *NN* interaction [27, 28] is given by

$$V_{ll'}^{full}(r, r') = W_{ll'}(r, r') + \delta(r - r')F_{ll'}^{cut}(r)V_{ll'}^{Yukawa}(r), \tag{9}$$

where,

$$F_{ll'}^{cut}(r) = \begin{cases} 1 - e^{-[\alpha_{ll'}(r-R_{ll'})]^2} & for \;\; r \geqslant R_{ll'} \\ 0 & for \;\; r \leqslant R_{ll} \end{cases}$$

$W_{ll'}(r, r')$ and $V_{ll'}^{Yukawa}(r)$ parts are the nonlocal and Yukawa tail (it is taken from AV18 potential [25]), respectively. The $F_{ll'}^{cut}(r)$ is the cut off function for the Yukawa tail. The $\alpha_{ll'}$ and $R_{ll'}$ are the fixed parameters which are 1.0 fm^{-1} and 2.0 fm, respectively. The nonlocal form $W_{ll'}(r, r')$ with parameters is given in [27]. These nonlocal INOY interactions are phenomenological and reproduce the 3*N* binding energies without adding a 3*N* force.

Apart from INOY, in the present work we use the interactions N3LO [29], $\text{N}^2\text{LO}_{opt}$ [43] and USDB [32]. The N3LO [29] is nucleon-nucleon interaction at the next-to-next-to-next-to-leading order (fourth order) of chiral perturbation theory (χPT). In this charge dependence is included up to next-to-leading order of the isospin-violation scheme. In χPT, the *NN* amplitude is uniquely determined by two classes of contributions: contact terms and pion-exchange diagrams. At N3LO, there are 24 parameters corresponding to 24 contact terms for the fitting of partial waves. The $\text{N}^2\text{LO}_{opt}$ [43] is optimized nucleon-nucleon interaction from chiral effective field theory at next-to-next-to-leading order (NNLO). Three pion-nucleon (πN) couplings (c_1, c_3, c_4) and 11 partial wave contact parameters C and $\tilde{C}$ were optimized. $\text{N}^2\text{LO}_{opt}$ interaction yields very good agreement with binding energies and radii for $A = 3, 4$ nuclei. $\text{N}^2\text{LO}_{opt}$ [43] is a bare interaction. In the bare interaction, the Okubo-Lee-Suzuki (OLS) [35, 36] transformation is not used. The USDB [32] interaction for shell model calculations with core is based on a renormalized G matrix with linear combinations of two-body matrix elements adjusted to fit a complete set of data for experimental binding energies and excitation energies for the *sd*-shell nuclei. This interaction was fitted by varying 56 linear combinations of parameters. This interaction is very successful to explain nuclear structure and nuclear astrophysical properties of *sd* shell nuclei.

The N3LO calculations are done at $\hbar\Omega = 14$ MeV. Previously, the NCSM calculations are done using N3LO *NN* interaction for ^{18}F up to $N_{\max} = 4$ [1]. In the present calculations we have reached up to $N_{\max} = 6$ in case of ^{18,19}F. The calculations with next-to-next leading order ($\text{N}^2\text{LO}_{opt}$) interaction at $\hbar\Omega$=20 MeV have been also reported. In the present calculations, we also see the difference between the results using bare and all other interactions (N3LO, INOY and USDB).

5. Results and discussions

We have performed the NCSM calculations for oxygen ($^{18-23}$O) and fluorine chains ($^{18-24}$F). NCSM calculations are variational which depend on $\hbar\Omega$ and size of model space $N_{\max}$. First we perform calculations with different frequencies for a given $N_{\max}$. We are interested in the region in which the dependence of g.s. energy on frequency is minimum (for largest model space). We select that frequency for NCSM calculations. This procedure is called optimization of frequency. When we use this frequency, we get faster convergence than other values of frequencies. This is the benefit of doing optimization of frequency. When we go to higher model space, the dependence on frequency decreases.

In figure 1 we have shown the variation of g.s. energies with the harmonic oscillator frequencies and different model space sizes for O isotopes. We can see the g.s. energy becomes less dependent when we move to higher $N_{\max}$. We obtain a minima at $\hbar\Omega = 20$ MeV. As we will go higher model space, we expect that this minima will shift at $\hbar\Omega = 18$ MeV. We pick up the frequency 18 and 20 MeV to perform NCSM calculations for the energy spectra. We have shown the energy spectra using different interactions for oxygen

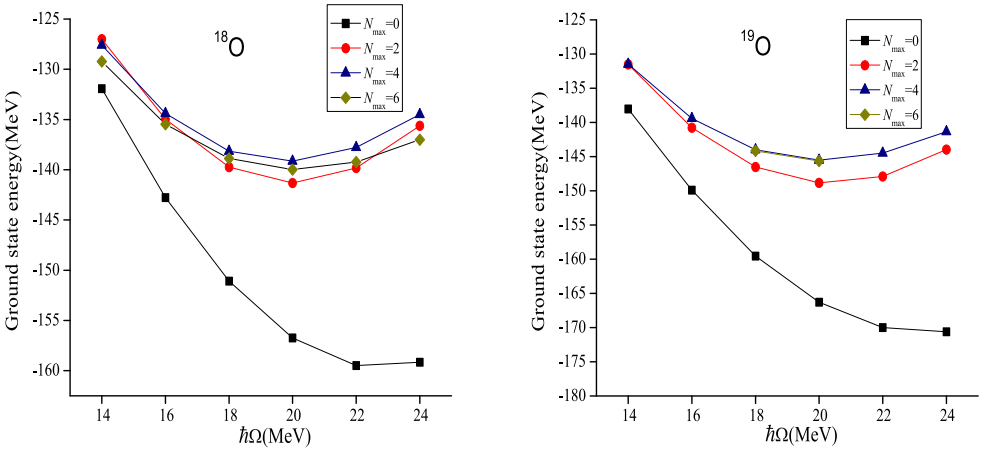

Figure 1. The variation of g.s. energy with frequencies at different model spaces for ^{18,19}O isotopes, similarly for other O isotopes.

chains in figures 2–3. We have also compared our NCSM results with phenomenological interaction USDB.

In the case of ^{18}O, as we move towards the higher $N_{\max}$ from 0 to 6, the calculated results also improve in comparison to lower $N_{\max}$ (however, 0_2^+ is at higher energy for $N_{\max} = 6$ in comparison with the lower $N_{\max}$). The gap between 0_1^+ and 2_1^+ increases smoothly as we move to higher $N_{\max}$. The results with $\hbar\Omega$=18 MeV are better than that of $\hbar\Omega$=20 MeV. At $\hbar\Omega$=18 MeV, the 2_1^+ and 4_1^+ states follow the same trend but the 0_2^+ and 2_2^+ states are in reverse order in comparison to the experimental data. This reverse order is also seen with USDB. In the case of ^{19}O, we are not getting the correct g.s. $5/2^+$ with both the frequencies. The calculated $5/2_2^+$ state is at higher energy. The calculated $9/2_1^+$ state is near to the experimental data. The first $1/2^+$ state is at higher energy in comparison with lower $N_{\max}$ results. In the case of ^{20}O, the low-lying spectra is in the correct order below energy $\sim$2.5 MeV for $N_{\max} = 6$. The 4_1^+ state is lower in energy compared to the experimental data. For ^{21}O, NCSM predicts g.s. as $5/2^+$ (although it is tentative experimentally). For ^{22}O, we get slightly better results than the lighter oxygen isotopes. Here, the states with NCSM calculations are in same order as in the experimental data. The states 0_2^+ and 3_1^+ are in reverse order with USDB interaction. The INOY interaction with $N_{\max} = 4$ calculations is not able to produce the large $N = 14$ shell gap, because 2_1^+ is at low-excitation energy, thus higher $N_{\max}$ calculations are needed. This correlation is also reflected from the predicted $1/2_1^+$, $3/2_1^+$ states in ^{21}O and $5/2_1^+$ in the^{23}O at low energy with $N_{\max} = 4$ calculations for INOY. For ^{23}O, we get the correct g.s. with NCSM. The calculated $5/2^+$ state is approaching towards the experimental $5/2^+$ state with increasing model space size.

For the first time we have reported NCSM results of ^{18,19,20,21}O isotopes for $N_{\max} = 6$. For ^{18,20}O our results show that as we go from $N_{\max} = 2$ to 6, there is a little improvement in the result of 2^+ and 4^+ states.

For F isotopes, we have shown the variation of g.s. energies with the harmonic oscillator frequencies and different model space sizes in figure 4, and energy spectra using different interactions in figures 5–8, respectively. We show the NCSM results using three interactions N3LO, INOY and N^{2}LO$_{opt}$ at $\hbar\Omega = 14$ MeV, 18 MeV and 20 MeV, respectively.

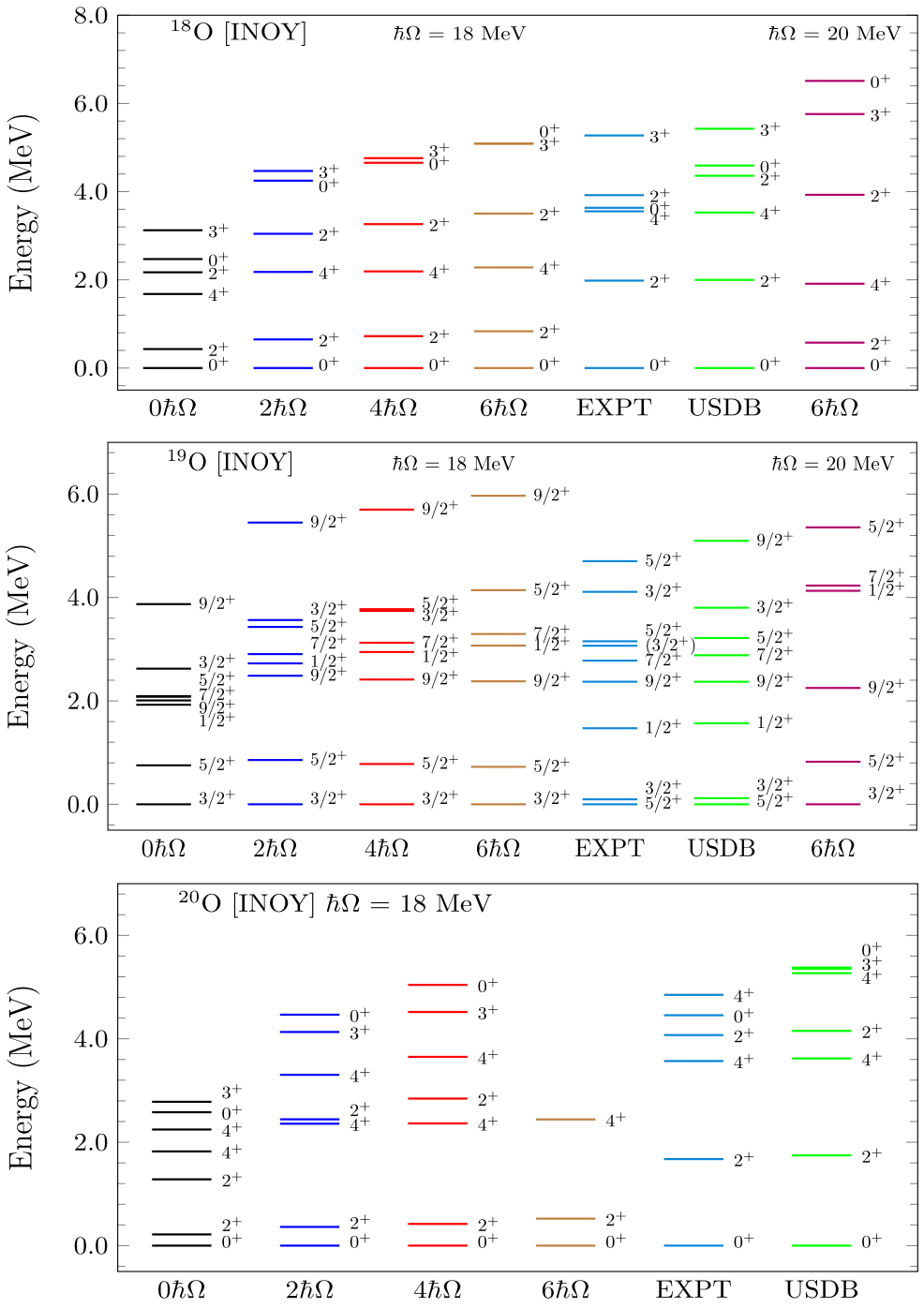

Figure 2. The energy spectra of $^{18-20}$O isotopes with INOY and USDB interactions.

For the F chain we have done calculations for $N_{\max} = 0$, 2, 4, and 6 (for ^{18,19}F) in the case of N3LO, while for INOY and N^{2}LO$_{opt}$ higher $N_{\max}$ calculations only. For ^{18}F (see figure 5), we can see that the NCSM calculations using N3LO interaction are better than

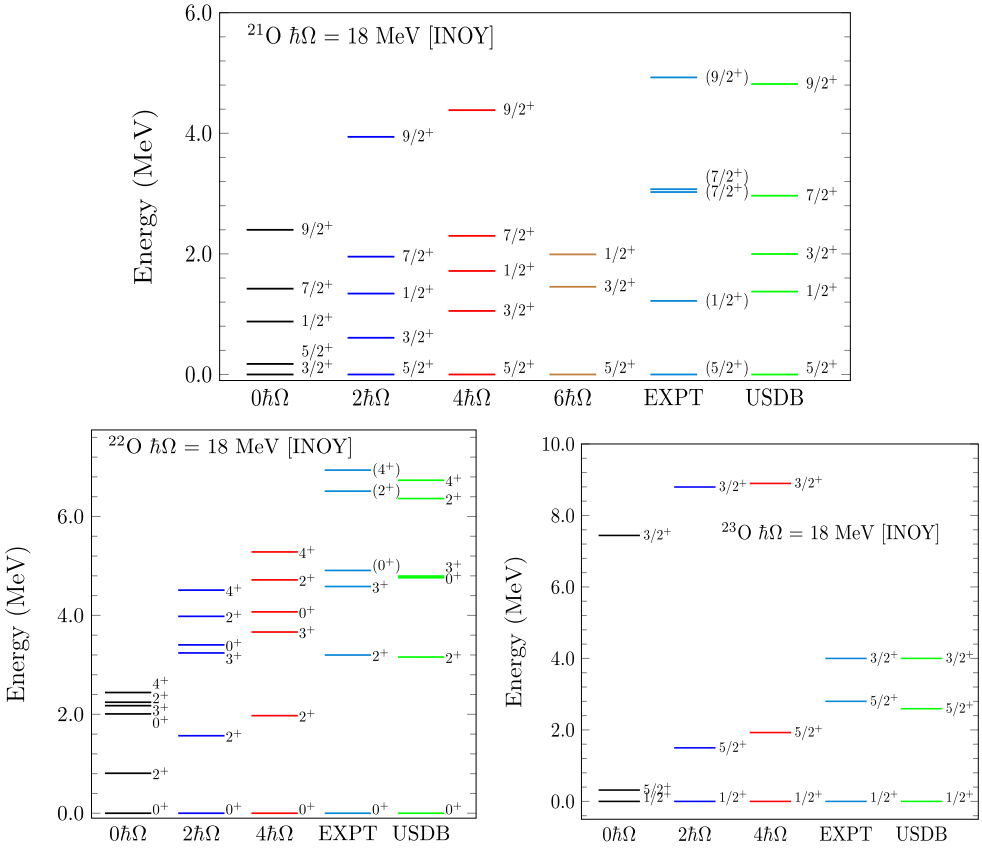

Figure 3. The energy spectra of $^{21-23}$O isotopes with INOY and USDB interactions.

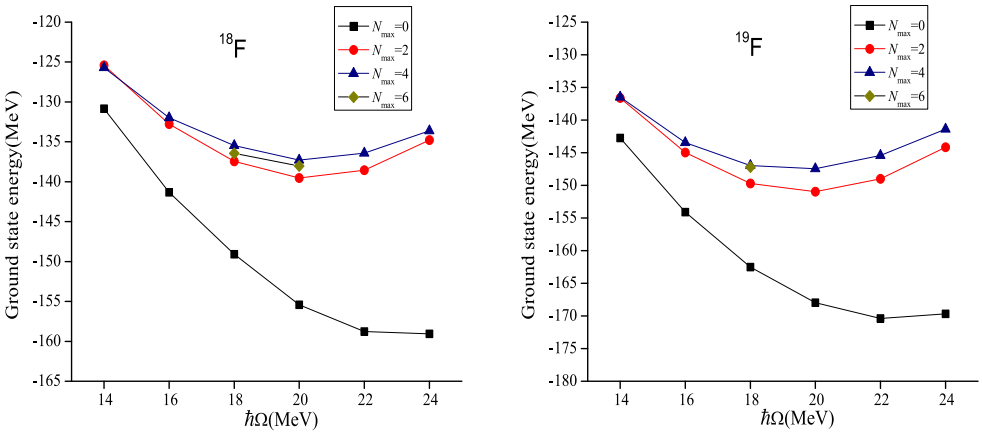

Figure 4. The variation of g. s. energy with frequencies at different model spaces for $^{18-19}$F isotopes, similarly for other F isotopes.

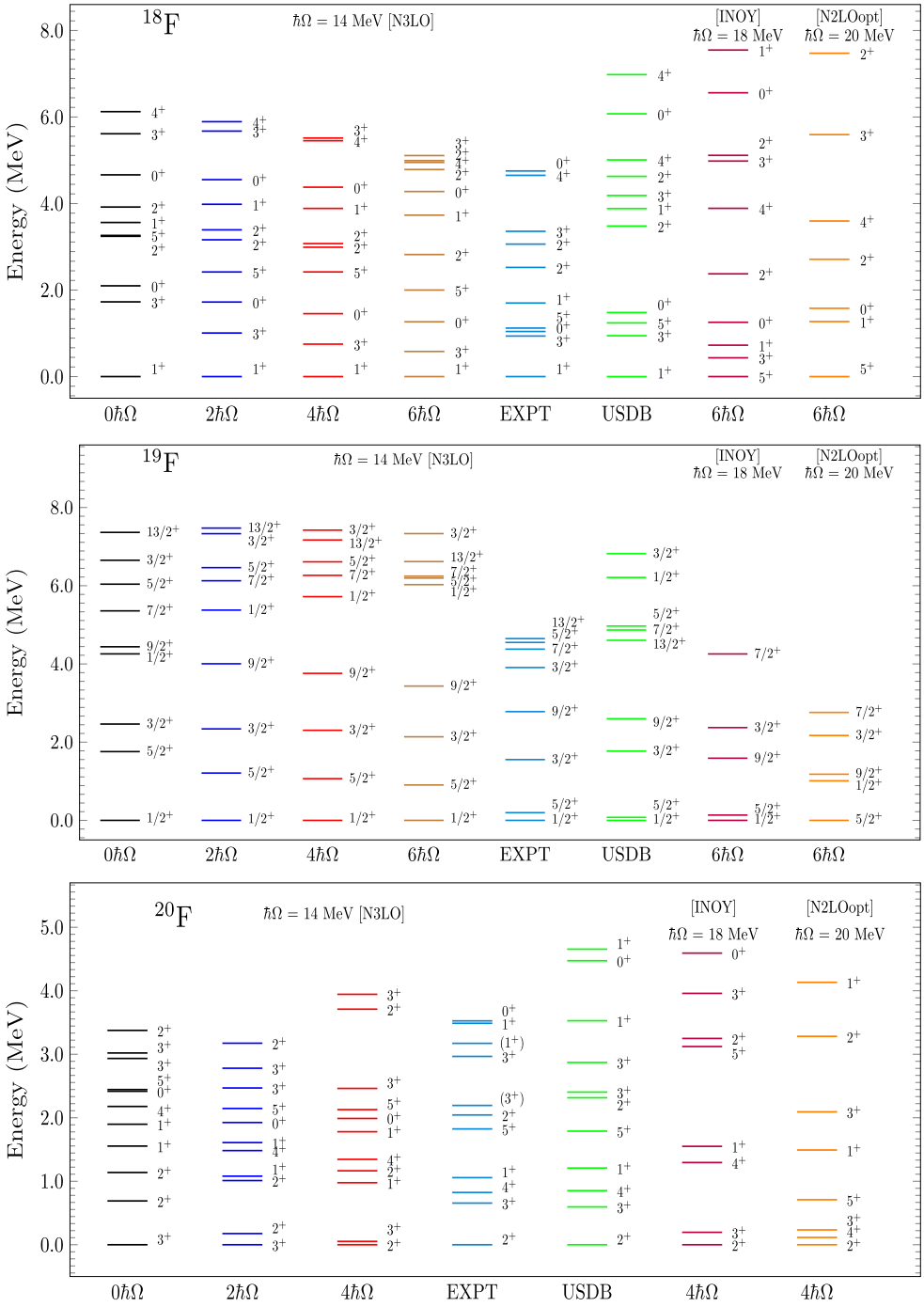

Figure 5. The energy spectra of $^{18-20}$F isotopes with N3LO, USDB, INOY and N^{2}LO$_{opt}$ interactions.

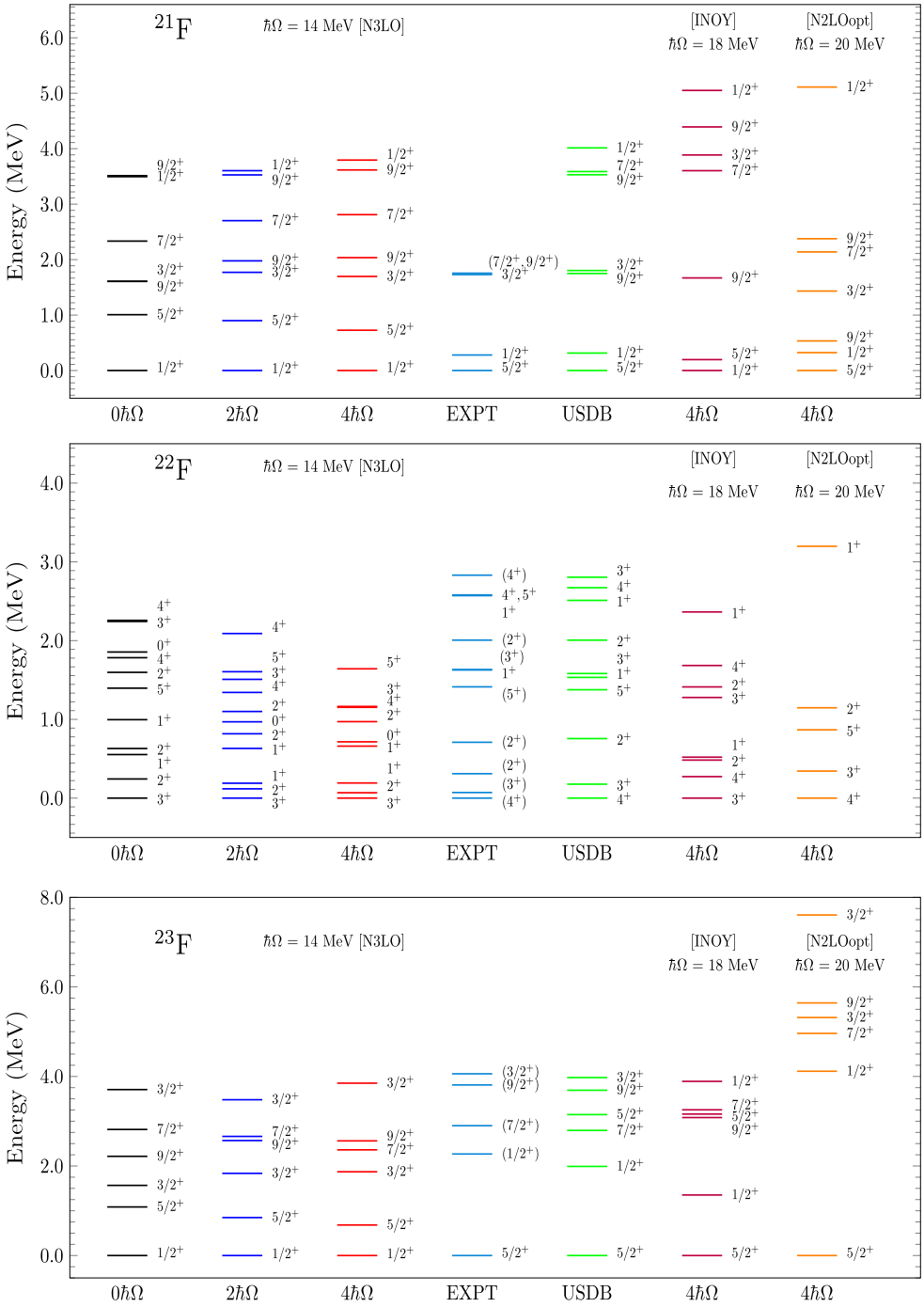

Figure 6. The energy spectra of $^{21-23}$F isotopes with N3LO, USDB, INOY and N^{2}LO$_{opt}$ interactions.

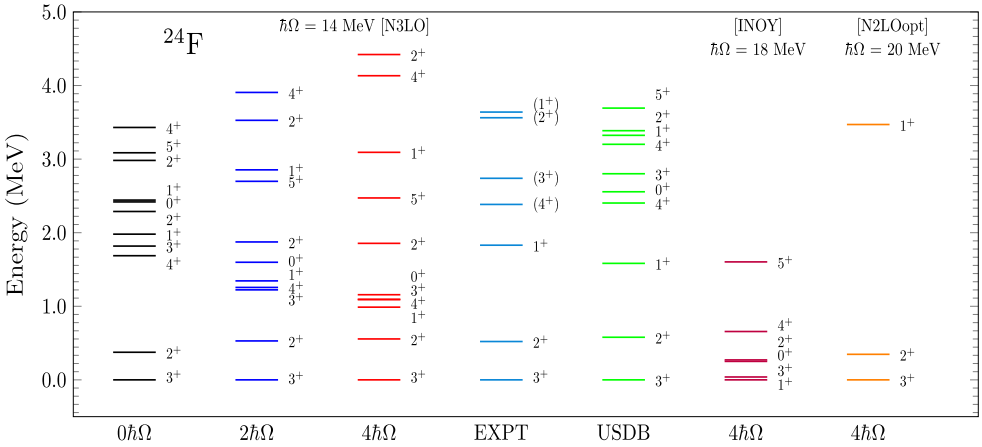

Figure 7. The energy spectra of ^{24}F isotope with N3LO, USDB, INOY and N^{2}LO$_{opt}$ interactions.

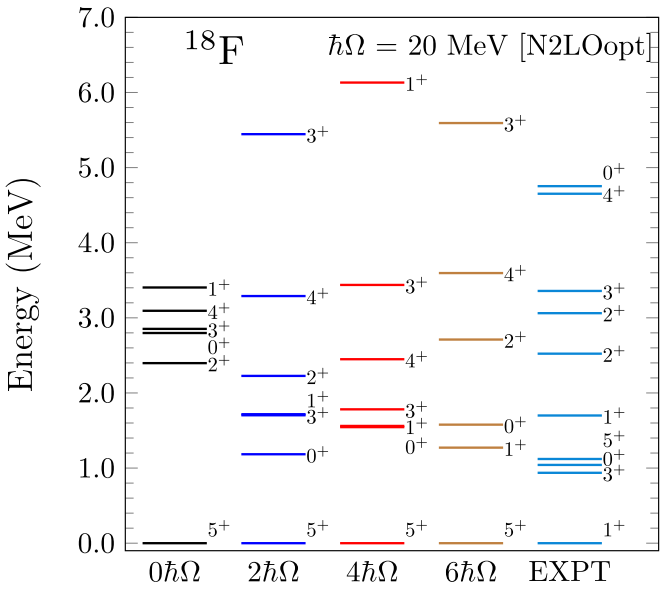

Figure 8. The energy spectra of ^{18}F with N^{2}LO$_{opt}$.

INOY and N^{2}LO$_{opt}$ interactions. The N3LO interaction predicts correct g.s. 1^+ while INOY and N^{2}LO$_{opt}$ fail to predict the correct ground state. The order of low-lying states up to 5^+_1 is correctly reproduced with the N3LO interaction while the other three interactions are not able to reproduce it correctly. The USDB interaction predicts 5^+_1 lower in comparison to 0^+_1. With N3LO, the calculated 0^+_1 state shows rapid convergence with increasing $N_{\max}$. The $N_{\max} = 6$ results are close to the experimental data. The calculated 0^+_2 state with N3LO is further compressed with increasing $N_{\max}$. The calculated value of 3^+_1 corresponding to $N_{\max} = 6$ is compressed in comparison to the experimental data. The difference between calculated and experimental excitation energy of 1^+_2 state is very large. To see the N^{2}LO$_{opt}$ results more systematically with different $N_{\max}$, we have shown corresponding results for ^{18}F in figure 8. The predicted 1^+ state is at high energy (>1 MeV) even with the $N_{\max} = 6$ calculation.

In case of ^{19}F, the $5/2_1^+$ state is close to the experimental data for INOY interaction and the order of $3/2_1^+$ and $9/2_1^+$ is reverse, while for the N3LO interaction the $5/2_1^+$ state is high in energy in comparison to the experimental data and it predicts the correct order for $3/2_1^+$ and $9/2_1^+$ states. With increasing $N_{\max}$ the excited states $5/2_1^+$-$3/2_1^+$-$9/2_1^+$ predicted by the N3LO interaction are showing fast convergence, while the gap between $9/2_1^+$-$1/2_2^+$ increases as $N_{\max}$ increases from 0 to 6. N^{2}LO$_{opt}$ interaction fails to reproduce the correct g.s. $1/2^+$. As we move from ^{18}F to ^{19}F, the INOY interaction results are much better.

From ^{20}F onwards, it is not possible to perform the NCSM calculation for $N_{\max} = 6$, thus we have reported results up to $N_{\max} = 4$ only. For ^{20}F, all three interactions reproduce the correct g.s. 2^+. The NCSM results using INOY interaction are better in comparison to N3LO and N^{2}LO$_{opt}$. The calculated 1_1^+ state with N3LO and USDB interactions is showing reasonable agreement with the experimental data.

In the case of ^{21}F, there is an inversion of the lowest $1/2^+$ and $5/2^+$ states in the spectra obtained from N3LO and INOY interactions in comparison with the experimental data. We need higher N$_{\max}$ calculations for these interactions because the $5/2^+$ state is converging very fast. In the case of ^{21}F and ^{22}F the N^{2}LO$_{opt}$ interaction reproduces the correct g.s. $5/2^+$ and 4^+, respectively. For ^{21}F, the NCSM results show a considerable gap between $9/2_1^+$ and $7/2_1^+$ states in comparison to the experimental data. Overall the N3LO prediction is not good for ^{22}F. It is clear that even if we do large $N_{\max}$ calculations our results will not be improved. For this isotope, the INOY interaction is also not able to predict the correct g.s.

In the case of ^{23}F, all the interactions (except N3LO) predict the correct g.s. as $5/2^+$. The $5/2^+$ state is converging very fast with INOY. Thus it is expected that if we do large $N_{\max}$ calculation then this interaction will be able to predict the correct g.s.

In the case of ^{24}F, except INOY, all other interactions predict the correct g.s. as 3^+. Thus, higher $N_{\max}$ calculations are needed for INOY. The first excited 2^+ state is predicted correctly with N3LO. The N3LO predicts 1_1^+ and 2_2^+ states at much lower energy in comparison with the experimental data. The 1^+ and 3^+ states are very close with the INOY interaction. If we do a higher $N_{\max}$ calculation for INOY then we get the correct g.s. as 3^+. The N^{2}LO$_{opt}$ interaction gives 1_1^+ state at very high energy. In the case of all fluorine isotopes we see the energy levels are more spread using the INOY interaction in comparison with the N3LO interaction. This is because of the strong $\tilde{\mathbf{l}}.\tilde{\mathbf{s}}$ coupling in the INOY interaction.

Overall, for better description of energy spectra in O and F chains we need to go to higher $N_{\max}$ calculations. Figure 9 shows the occupancies for the ground and first excited states for the even oxygen and fluorine chains, respectively. We have shown the occupation numbers up to the *fp* shell. Above the *fp* shell the occupation numbers are very small and very hard to visualize (in the present figure). So, we have not shown the orbitals beyond the *fp* shell. The occupancy of the $\nu d_{5/2}$ orbital is increasing from ^{18}O to ^{24}O. For ^{24}O, the occupancy of the $\nu d_{3/2}$ orbital shows significant increase from 0_1^+ to 2_1^+ state, while $\nu s_{1/2}$ occupancy is decreasing.

In figure 10 we have shown ^{18}O point-proton radius as a function of $\hbar\Omega$ obtained with the INOY interaction. The crossing point of the INOY curves suggests that the $r_p \approx 2.12$ fm at 18 $\hbar\Omega$, while the corresponding experimental value is 2.68(10) fm.

6. Location of drip line in oxygen isotopes

As we know from the previous work in the oxygen chain, the 3N forces are needed to reproduce the drip line at ^{24}O [24, 44, 45]. The calculations were previously done [24, 44, 45]

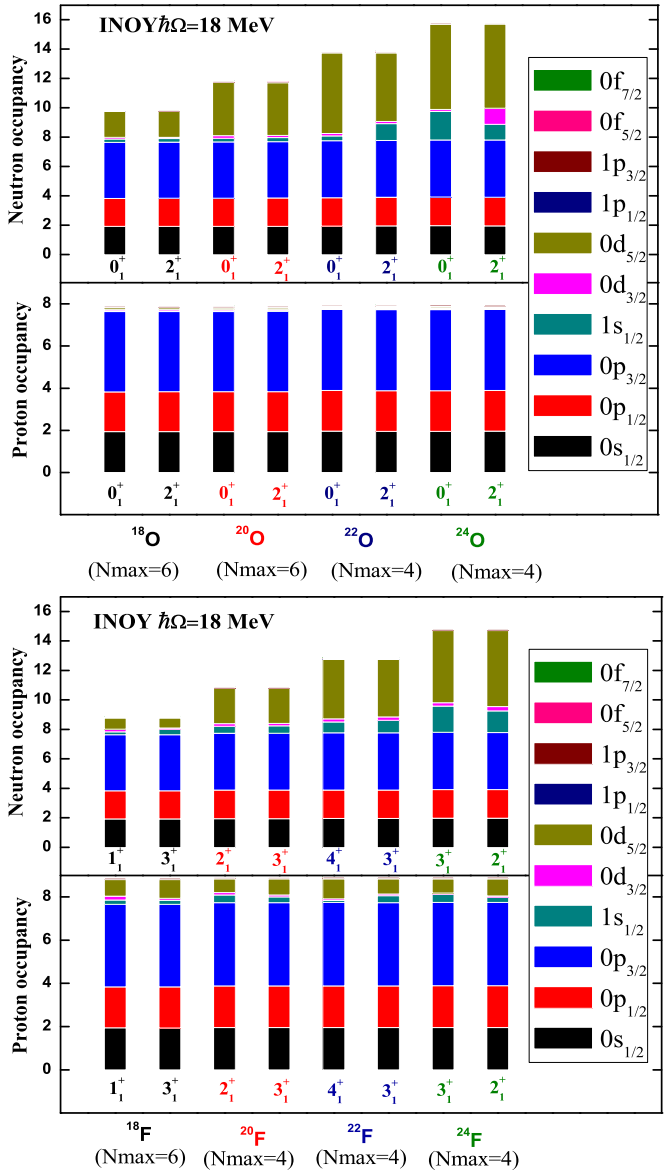

Figure 9. Systematics of occupation numbers for even O and F isotopes.

using chiral *NN*, *NN* + *NNN*-induced and *NN* + *NNN*-full interactions. The anomalous behaviour in oxygen isotopes can be explained only after adding 3N forces. The *NN* interaction shows the drip line at ^{28}O [23, 24, 46]. In the present work, we have applied the INOY *NN* interaction which has the effect of three-body forces in terms of short range and non-locality character present in it and it also reproduces the correct binding energy of triton. In the upper panel of figure 11, we have shown the g.s. energies for oxygen isotopes using INOY at $\hbar\Omega = 18$MeV. The g.s. energy decreases as we reach ^{24}O but we see a kink after this. This shows the drip line in oxygen isotopes at ^{24}O. The g.s. energy for fluorine isotopes is shown in the lower panel of figure 11. Using INOY interaction the g.s energies are quite

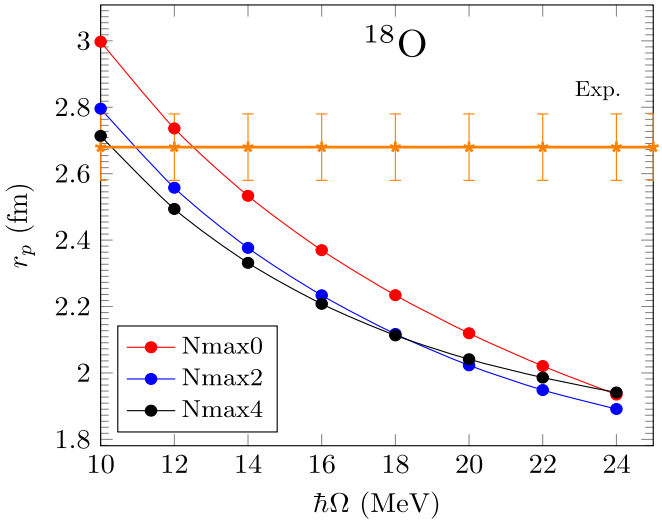

Figure 10. ^{18}O point-proton radius as a function of $\hbar\Omega$ obtained with INOY interaction in NCSM calculations for $N_{\max} = 0$, 2, and 4. The experimental value with uncertainties [47] is also shown.

good up to ^{21}F. We have extrapolated the g.s. energy using an exponential fitting function $E_{g.s.}(N_{\max}) = a\ \ exp(-bN_{\max}) + E_{g.s.}(\infty)$ with $E_{g.s.}(\infty)$ the value of g.s. energy at $N_{\max} \to \infty$ for $^{18-21}$O using $N_{\max} = 0$, 2, 4 and 6 results, while beyond ^{21}O $N_{\max} = 0$, 2, and 4 results only.

The location of drip line for O and F chain using hybrid *ab initio* approach is reported by Tichai *et al* in [23]. In this work [23] low-lying spectra of ^{18,19,20}O isotopes up to $N_{\max} = 6$ are also reported. Otsuka *et al*, previously reported first microscopic explanation of the oxygen anomaly based on three-nucleon forces in [24].

7. Conclusions

In the present work, for the first time we have reported no-core shell model results of oxygen and fluorine chains using the INOY *NN* interaction. This is also the first time we have done NCSM calculations for larger $N_{\max}$ (up to $N_{\max} = 6$ for some isotopes) for O and F chains. The NCSM study with the INOY *NN* interaction is very important because it gives the effect of three-body forces without adding three-body forces explicitly. We have reported energy spectra for positive parity states and neutron and proton occupancies for the maximum reached $N_{\max}$ in our calculations. The NCSM calculations with INOY interaction predict correctly the drip line at ^{24}O for oxygen chain. The large $N = 14$ shell gap is not reproduced with INOY interaction. However, if we perform higher $N_{\max}$ calculations with INOY interaction then it is possible to get large $N = 14$ shell gap. The INOY interaction is unable to correctly reproduce the experimental data for the ^{18}F isotope, however as we move to heavier neutron rich F isotopes the results are in a reasonable agreement with the experimental data in comparison to N3LO and N^{2}LO$_{opt}$ interactions.

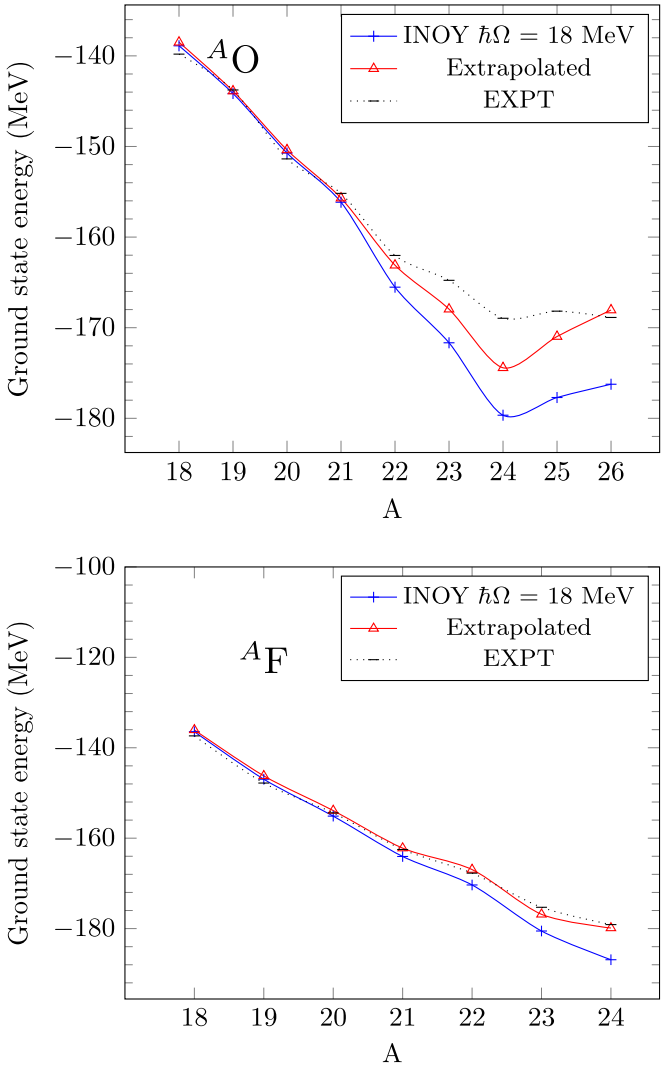

Figure 11. Comparison of experimental, calculated (corresponding to $\hbar\Omega = 18$ MeV) and extrapolated g.s. energies of O and F isotopes with INOY interaction. For $^{18-21}$O and ^{18,19}F the g.s. energy is for $N_{\max} = 6$ and for rest isotopes with $N_{\max} = 4$.

Acknowledgments

We would like to thank Prof. Petr Navrátil for providing us his NN effective interaction code and for his valuable comments and suggestions from the beginning of this project. Thanks are also due to Prof. Christian Forssén for pANTOINE and for several discussions. AS acknowledges financial support from MHRD (Govt. of India) for her PhD thesis work. We acknowledge Oak computational facility at TRIUMF for No-Core Shell Model calculations. P.C.S. acknowledges the hospitality extended to him during his stays at TRIUMF in the summer of 2016 and 2018. PCS acknowledges a research grant from SERB (India), CRG/2019/000556.

ORCID iDs

Praveen C Srivastava https://orcid.org/0000-0001-8719-1548

References

[1] Barrett B R, Navrátil P and Vary J P 2013 *Ab initio* no-core shell model *Prog. Part. Nucl. Phys.* **69** 131–81
[2] Navrátil P, Vary J P and Barrett B R 2000 Properties of ^{12}C in the *ab initio* nuclear shell model *Phys. Rev. Lett.* **84** 5728
[3] Navrátil P, Vary J P and Barrett B R 2000 Large-basis *ab initio* no-core shell model and its application to ^{12}**C** *Phys. Rev.* C **62** 054311
[4] Navrátil P, Quaglioni S, Stetcu I and Barrett B R 2009 Recent developments in no-core shell-model calculations *J. Phys.* G **36** 08310
[5] Forssén C, Roth R and Navrátil P 2013 Systematics of 2^+ states in C isotopes from the no-core shell model *J. Phys. G: Nucl. Part. Phys.* **40** 055105
[6] Saxena A and Srivastava P C 2019 *Ab initio* no-core shell model study of neutron-rich nitrogen isotopes *Prog. Theor. Exp. Phys.* **2019** 073D02
[7] Soma V, Navrátil P, Raimondi F, Barbieri C and Duguet T 2020 Novel chiral Hamiltonian and observables in light and medium-mass nuclei *Phys. Rev.* C **101** 014318
[8] Shirokov A M, Vary J P, Mazur A I and Weber T A 2007 Realistic nuclear Hamiltonian: ab exitu approach *Phys. Lett.* B **644** 33
[9] Shirokov A M, Shin I J, Kim Y, Sosonkina M, Maris P and Vary J P 2016 N3LO NN interaction adjusted to light nuclei in ab exitu approach *Phys. Lett.* B **761** 87
[10] Baroni S, Navrátil P and Quaglioni S 2013 *Ab initio* description of the exotic unbound ^{7}He Nucleus *Phys. Rev. Lett.* **110** 022505
[11] Baroni S, Navrátil P and Quaglioni S 2013 Unified *ab initio* approach to bound and unbound states: No-core shell model with continuum and its application to ^{7} He *Phys. Rev.* C **87** 034326
[12] Navrátil P, Quaglioni S, Hupin G, Romero-Redondo C and Calci A 2016 Unified *ab initio* approaches to nuclear structure and reactions *Phys. Scr.* **91** 053002
[13] Calci A, Navrátil P, Roth R, Dohet-Eraly J, Quaglioni S and Hupin G 2016 Can *ab initio* theory explain the phenomenon of parity inversion in ^{11}Be? *Phys. Rev. Lett.* **117** 242501
[14] Forssén C, Navrátil P, Ormand W E and Caurier E 2005 Large basis *ab initio* shell model investigation of ^{9}Be and ^{11}Be *Phys. Rev.* C **71** 044312
[15] Dikmen E, Lisetskiy A F, Barrett B R, Maris P, Shirokov A M and Vary J P 2015 *Ab initio* effective interactions for sd-shell valence nucleons *Phys. Rev.* C **91** 064301
[16] Smirnova N A, Barrett B R, Kim Y, Shin I J, Shirokov A M, Dikmen E, Maris P and Vary J P 2019 Effective interactions in the sd shell *Phys. Rev.* C **100** 054329
[17] Saxena A and Srivastava P C 2017 First-principles results for electromagnetic properties of sd shell nuclei *Phys. Rev.* C **96** 024316
[18] Saxena A, Srivastava P C and Suzuki T 2018 *Ab initio* calculations of Gamow-Teller strengths in the sd shell *Phys. Rev.* C **97** 024310
[19] Saxena A, Kumar A, Kumar V, Srivastava P C and Suzuki T 2019 Ab initio description of collectivity for sd shell nuclei *Hyperfine Interact.* **240** 37
[20] Ruotsalainen P *et al* 2019 Isospin symmetry in $B(E2)$ values: Coulomb excitation study of ^{21}Mg *Phys. Rev.* C **99** 051301(R)
[21] Williams J *et al* 2019 Structure of ^{28}Mg and influence of the neutron pf shell *Phys. Rev.* C **100** 014322
[22] Stroberg S R, Hergert H, Holt J D, Bonger S K and Schwenk A 2016 Ground and excited states of doubly open-shell nuclei from *ab initio* valence-space Hamiltonians *Phys. Rev.* C **93** 051301(R)
[23] Tichai A, Gebrerufael E, Vobig K and Roth R 2018 Open-shell nuclei from no-core shell model with perturbative improvement *Phys. Lett.* B **786** 448
[24] Otsuka T, Suzuki T, Holt J D, Schwenk A and Akaishi Y 2010 Three-body forces and the limit of oxygen isotopes *Phys. Rev. Lett.* **105** 032501
[25] Wiringa R B, Stoks V G J and Schiavilla R 1995 Accurate nucleon-nucleon potential with charge-independence breaking *Phys. Rev.* C **51** 38

[26] Machleidt R 2001 High-precision, charge-dependent Bonn nucleon-nucleon potential *Phys. Rev.* C **63** 024001
[27] Doleschall P and Borbély I 2000 Properties of the nonlocal NN interactions required for the correct triton binding energy *Phys. Rev.* C **62** 054004
[28] Doleschall P, Borbély I, Papp Z and Plessas W 2003 Nonlocality in the nucleon-nucleon interaction and three-nucleon bound states *Phys. Rev.* C **67** 064005
[29] Entem D R and Machleidt R 2003 Accurate charge-dependent nucleon-nucleon potential at fourth order of chiral perturbation theory *Phys. Rev.* C **68** 041001(R)
[30] Bogner S K, Kuo T T S and Schwenk A 2003 Model-independent low momentum nucleon interaction from phase shift equivalence *Phys. Rept.* **386** 1
[31] Bogner S K, Furnstahl R J and Perry R J 2007 Similarity renormalization group for nucleon-nucleon interactions *Phys. Rev.* C **75** 061001(R)
[32] Brown B A and Richter W A 2006 New USD Hamiltonians for the sd shell *Phys. Rev.* C **74** 034315
[33] Navrátil P and Barrett B R 1996 No-core shell-model calculations with starting-energy-independent multivalued effective interactions *Phys. Rev.* C **54** 2986
[34] Navrátil P, Vary J P and Barrett B R 2000 Large-basis ab initio no-core shell model and its application to ^{12}C *Phys. Rev.* C **62** 054311
[35] Suzuki K and Lee S Y 1980 Convergent theory for effective interaction in nuclei *Prog. Theor. Phys.* **64** 2091
[36] Suzuki K 1982 Construction of Hermitian effective interaction in nuclei: - general relation between Hermitian and Non-Hermitian forms *Prog. Theor. Phys.* **68** 246
[37] Gloeckner D H and Lawson R D 1974 Spurious center-of-mass motion *Phys. Lett.* B **53B** 313
[38] Forssén C, Carlsson B D, Johansson H T and Sääf D 2018 Large-scale exact diagonalizations reveal low-momentum scales of nuclei *Phys. Rev.* C **97** 034328
[39] Caurier E and Nowacki F 1999 Present status of shell model techniques *Acta Phys. Pol.* B **30** 705
[40] Caurier E, Martínez-Pinedo G, Nowacki F, Poves A, Retamosa J and Zuker A P 1999 Full $0\hbar\omega$ shell model calculation of the binding energies of the $1f_{7/2}$ nuclei *Phys. Rev.* C **59** 2033
[41] Caurier E, Navrátil P, Ormand W E and Vary J P 2001 Intruder states in ^{8}Be *Phys. Rev.* C **64** 051301(R)
[42] Polyzou W and Glöckle W 1990 Three-body interactions and on-shell equivalent two-body interactions *Few-Body Syst.* **9** 97
[43] Ekström A *et al* 2013 Optimized chiral nucleon-nucleon interaction at next-to-next-to-leading order *Phys. Rev. Lett.* **110** 192502
[44] Hagen G, Hjorth-Jensen M, Jansen G R, Machleidt R and Papenbrock T 2012 Continuum effects and three-Nucleon forces in neutron-rich oxygen isotopes *Phys. Rev. Lett.* **108** 242501
[45] Cipollone A, Barbieri C and Navrátil P 2013 Isotopic chains around oxygen from evolved chiral two- and three-nucleon interactions *Phys. Rev. Lett.* **111** 062501
[46] Hergert H, Binder S, Calci A, Langhammer J and Roth R 2013 Ab initio calculations of even oxygen isotopes with chiral two-plus-three-nucleon interactions *Phys. Rev. Lett.* **110** 242501
[47] Lapoux V, Soma V, Barbieri C, Hergert H, Holt J D and Stroberg S R 2016 Radii and binding energies in oxygen isotopes: a challenge for nuclear forces *Phys. Rev. Lett.* **117** 052501